Open Archive TOULOUSE Archive Ouverte (OATAO)

A novel method for detecting and computing univolatility curves in ternary mixtures

Nataliya Shcherbakova [a], Ivonne Rodriguez-Donis [b,*], Jens Abildskov [b], Vincent Gerbaud [c]

[a] Laboratoire de Génie Chimique, Université Paul Sabatier – INP ENSIACET, 4, allée Emile Monso, 31432 Toulouse, France
[b] CAPEC-PROCESS, Department of Chemical and Biochemical Engineering, Technical University of Denmark, Building 229, DK-2800 Kgs. Lyngby, Denmark
[c] Laboratoire de Génie Chimique, CNRS, 4, allée Emile Monso, CS 84234, 31432 Toulouse, France

---

HIGHLIGHTS

- 3D generalized univolatility surfaces are defined.
- Ternary RCM univolatility curves are the loci of relative composition critical points.
- Ordinary differential equations describe the univolatility curves.
- A new algorithm based on an initial value problem is proposed.
- The method finds univolatility curves not connected to any azeotrope.

ABSTRACT

Residue curve maps (RCMs) and univolatility curves are crucial tools for analysis and design of distillation processes. Even in the case of ternary mixtures, the topology of these maps is highly non-trivial. We propose a novel method allowing detection and computation of univolatility curves in homogeneous ternary mixtures independently of the presence of azeotropes, which is particularly important in the case of zeotropic mixtures. The method is based on the analysis of the geometry of the boiling temperature surface constrained by the univolatility condition. The introduced concepts of the generalized univolatility and unidistribution curves in the three dimensional composition – temperature state space lead to a simple and efficient algorithm of computation of the univolatility curves. Two peculiar ternary systems, namely diethylamine – chloroform – methanol and hexane – benzene – hexafluorobenzene are used for illustration. When varying pressure, tangential azeotropy, bi-ternary azeotropy, saddle-node ternary azeotrope, and bi-binary azeotropy are identified. Moreover, rare univolatility curves starting and ending on the same binary side are found. In both examples, a distinctive crossing shape of the univolatility curve appears as a consequence of the existence of a common tangent point between the three dimensional univolatility hypersurface and the boiling temperature surface.

---

1. Introduction

Separation of liquid mixtures is one of the most important tasks in the process industry where distillation is the most widely used technique. Remarkably, almost every product on the market contains chemicals that have undergone distillation (Kiss, 2014). Beyond conventional distillation of binary and multi-component mixtures, several additional distillation techniques are developed for breaking azeotropes or separating close boiling mixtures: pressure swing distillation, azeotropic and extractive distillation. These techniques are covered at length in several textbooks and reviews (Skiborowski et al., 2014; Gerbaud and Rodriguez-Donis, 2014; Arlt, 2014; Olujic, 2014).

Preliminary conceptual design of distillation processes is based on the knowledge of the mixture thermodynamics and on the analysis of the residue curve maps (RCMs). RCMs are useful to assess the feasibility of splits since they approximate the column composition profiles under total reflux (Doherty and Malone, 2001; Petlyuk, 2004). RCMs also display azeotropes and distillation boundaries, as well as unidistribution and univolatility manifolds. These geometrical concepts have been reviewed in several works. Particularly, the review paper of Kiva et al. (2003) provides a comprehensive historical review of RCMs mainly taking into account

* Corresponding author.
  E-mail address: ivonnerd02@gmail.com (I. Rodriguez-Donis).

the Serafimov's classification of 26 RCM diagrams of ternary systems (Hilmen et al.,2002). The important role of RCMs, unidistribution and univolatility manifolds has been well described by Widagdo and Seider (1996), Ji and Liu (2007), Skiborowski et al. (2014) for azeotropic distillation process design and by Rodriguez-Donis et al. (2009a, 2009b, 2012a, 2012b), Luyben and Chien (2010) and Petlyuk et al. (2015) for extractive distillation design purposes. Noteworthy, the existence and the position of the univolatility curve, a particular type of isovolatility curve, determine the component to be drawn as distillate as well as the configuration of the extractive distillation column.

Isovolatility curves are curves along which the relative volatility of a pair of species is constant:

$$\alpha_{ij} = \frac{y_i/x_i}{y_j/x_j} = constant, \quad i \neq j$$

Along *univolatility* curves $\alpha_{ij} = 1$. As their properties are closely related to those of residue curves (Kiva et al., 2003), univolatility, isovolatility, and isodistribution curves are useful for studying the feasibility of distillation processes. For example, the most volatile component is likely to be recovered in the distillate stream with the so-called direct split whereas the least volatile is likely to be in the bottom stream with the so-called indirect split. In azeotropic and extractive distillation processes an entrainer is added to the liquid mixture to be separated, in order to enhance the relative volatility between the components. If the isovolatility rate increases towards the entrainer vertex, it is a good indicator of an easy separation (Laroche et al., 1991; Wahnschafft and Westerberg, 1993; Luyben and Chien, 2010). Furthermore in extractive distillation, the location of the univolatility curve and its intersection with the composition triangle edge determine the component to be withdrawn as a distillate product from the extractive column as well as the proper column configuration (Laroche et al., 1991; Lelkes et al., 1998; Gerbaud and Rodriguez-Donis, 2014).

As shown by Kiva and Serafimov (1973), univolatility curves divide the composition space, Ω, into different K-order regions. Zhvanetskii et al. (1988) proposed the main principles describing all theoretically possible structures of univolatility curves for zeotropic ternary mixtures and their respective location according to the thermodynamic relationship between the distribution coefficients of the light component i, the intermediate j and the heavy component m. 33 possible structures of univolatility curves were reported under the assumption that for every pair of components there exists only one univolatility curve. In the succeeding paper from the same group (Reshetov et al., 1990), the classification was refined by introducing the following nomenclature:

– $\overline{\alpha_{i,j}}$: an arc shape univolatility curve whose terminal points belong to the same binary side of the composition triangle;
– $\overline{\overline{\alpha_{i,j}}}$: the univolatility curve connecting two different binary sides of the composition triangle.

Later Reshetov and Kravchenko (2010) extended their earlier analysis to ternary mixtures having at least one binary azeotrope. Their main observations are:

(a) more than one univolatility curve having the same component index "i,j" can appear in a ternary diagram;
(b) the univolatility curve that does not start at the binary azeotrope can be either $\overline{\alpha_{i,j}}$ or $\overline{\overline{\alpha_{i,j}}}$ type. An $\overline{\alpha_{i,j}}$ curve can cross a separation boundary of the RCM;
(c) a ternary azeotrope can be crossed by any type of univolatility curve;

(d) if two univolatility curves intersect at some point, this point is a tangential binary azeotrope or a ternary azeotrope. In both cases there is a third univolatility curve of complementary type passing through this point;
(e) transitions from $\overline{\alpha_{i,j}}$ to $\overline{\overline{\alpha_{i,j}}}$ (or vice versa) can occur as univolatility curves depend on pressure and temperature of vapor – liquid equilibrium (VLE).

Despite the increasing application of univolatility curves in conceptual design, there still lacks a method allowing:

(1) detection of the existence of univolatility curves independently of the presence of azeotropes, which is particularly important in the case of zeotropic mixtures;
(2) simple and efficient computation of univolatility curves.

In fact, numerical methods available in most chemical process simulators allow mainly the computation of the univolatility curves linked to azeotropic compositions. Missing univolatility curves not connected to azeotropes will result in improper design of the extractive distillation process. This problem can be solved by a fully iterative searching in the ternary composition space providing the composition values with equal relative volatility (Bogdanov and Kiva, 1977). Skiborowski et al. (2016) have recently proposed a method to detect the starting point of the univolatility curve. They locate all pinch branches that bifurcate when moving from the pure component vertex along the corresponding binary sides. The robustness of this approach to handle complex cases, such as biazeotropy when more than one univolatility curve ends on the same binary side, is well demonstrated. Their algorithm is based on MESH equations, including mass and energy balances, summation constraints, and equilibrium conditions.

A less tedious and less time-consuming method is proposed in this paper. It is based on the geometry of the boiling temperature surface constrained by the univolatility condition. This approach will also require the computation of starting binary compositions independently of the azeotrope condition. Such starting points can be easily computed with a vapor-liquid equilibrium model by using the intersections of the distribution coefficient curves on each binary side of the ternary diagram (Kiva et al., 2003).

This paper is organized as follows: First, we revisit the properties of the univolatility curves in RCMs, and prove that they are formed by critical points of the relative compositions. Then, we show that the topology of unidistribution and univolatility curves follows from both the global geometrical structure of the boiling temperature surface and the univolatility condition considered in the full three-dimensional composition - temperature state space. Such a consideration leads to a simple algorithm for the numerical computation of the univolatility curves and other similar objects by solving a system of ordinary differential equations. The starting points of the univolatility curves computation can be detected from the relationship between the distribution coefficients related to the binary pair "i,j": the binary distribution coefficients $k_i^{i,j}$, $k_j^{i,j}$ and the ternary coefficient $k_m^{\infty i,j}$ describing the ternary mixture with the third component "m" at infinite dilution. Finally, we illustrate our approach by considering several topological configurations of RCM for two distinctive ternary mixtures (thermodynamic model parameters for both mixtures are available online as the supplementary material to this article). The ternary mixture diethylamine – chloroform – methanol at different pressures has two univolatility curves with the same component index "i,j" and one univolatility curve of type $\overline{\overline{\alpha_{i,j}}}$. We also applied our method to the well-known (though uncommon) case of the binary mixture benzene – hexafluorobenzene exhibiting two azeotropes at

atmospheric pressure. Considering hexane as the third component of the ternary mixture, we trace out the transformation of the type of the univolatility curve from $\overline{\overline{\alpha_{i,j}}}$ to $\overline{\alpha_{i,j}}$ with the variation of pressure. The transformation of the topological structure of the univolatility curves is properly computed by using the new computational method.

2. Methodology

2.1. Basic definitions and notations

Consider an open evaporation of a homogeneous ternary mixture at thermodynamic equilibrium of the vapor and liquid phases at constant pressure. Let $x_i, y_i, \ i = 1, 2, 3$ denote the mole fractions in the liquid and in the vapor phases. T is the absolute temperature of the mixture. Since $x_1 + x_2 + x_3 = 1$, only two mole fractions are independent. Selecting (arbitrarily) x_1 and x_2, the possible compositions of the liquid belong to the *Gibbs triangle* $\Omega = \{(x_1, x_2): \ x_i \in [0, 1], \ i = 1, 2\}$, and we denote by $\partial\Omega$ its boundary. In what follows we will use the vector notation $\bar{x} = (x_1, x_2)$. According to the phase rule - in the absence of chemical reactions - a two-phase ternary mixture has three independent state variables. If we select x_1, x_2 and T, the complete state space of a ternary mixture is the set

$$\{(\bar{x}, T): \ T \in [T_{min}, T_{max}], \quad \bar{x} \in \Omega, \quad i = 1, 2\}$$

Here T_{min}, T_{max} are the minimum and maximum boiling temperatures of the mixture. Throughout this paper we assume the vapor phase ideality, i.e. at constant pressure the vapor phase is related to the liquid phase through an appropriate thermodynamic model of the form $y_i = K_i(x_1, x_2, T)x_i, \ i = 1, 2, 3$. The functions K_i are the *distribution coefficients*. The liquid mixture of a given composition $\bar{x}$ has a corresponding boiling temperature, which can be computed from the thermodynamic equilibrium equation:

$$\Phi(x_1, x_2, T) = \sum_{i=1}^{3} y_i - 1 = \sum_{i=1}^{3} K_i(x_1, x_2, T)x_i - 1 = 0 \qquad (1)$$

The *boiling temperature surface*, defined by Eq. (1), can be interpreted geometrically as a hypersurface in three-dimensional space. We will denote it by W. In a homogeneous mixture each composition of the liquid phase is characterized by an unique value of T, so $\frac{\partial\Phi(\bar{x}, T)}{\partial T} \neq 0$ for any $T \in [T_{min}, T_{max}]$ and $\bar{x} \in \Omega$. This allows application of the Implicit Function Theorem (Lang, 1987) to solve Eq. (1). Thus, in principle, the boiling temperature can be computed as a function of the composition: $T = T_b(x_1, x_2)$. Hence, in the three dimensional state space the boiling temperature surface can be represented as a graph of the function $T_b(x_1, x_2)$. Moreover, by construction, $\Phi(x_1, x_2, T_b(x_1, x_2)) \equiv 0$, so the gradient of the function $T_b(x_1, x_2)$ can be computed explicitly:

$$\frac{\partial T_b}{\partial x_1} = -\frac{\frac{\partial\Phi}{\partial x_1}}{\frac{\partial\Phi}{\partial T}}, \quad \frac{\partial T_b}{\partial x_2} = -\frac{\frac{\partial\Phi}{\partial x_2}}{\frac{\partial\Phi}{\partial T}} \qquad (2)$$

In the standard equilibrium model of open evaporation, a multicomponent liquid mixture is vaporized in a still in such a way that the vapor is continuously evacuated from the system. Transient mass balances imply

$$\dot{x}_i = x_i - y_i(x_1, x_2, T), \quad i = 1, 2, \qquad (3)$$

the derivatives in Eq. (3) is computed with respect to some dimensionless parameter ξ (Doherty and Malone, 2001). The solutions of the system of DAEs (1) + (3) define certain curves on the boiling temperature surface W, whose projections on Ω are called the *residue curves*. The complete set of such curves forms the RCM.

The right hand sides of (3) define a vector field $\bar{v} = (x_1 - y_1, x_2 - y_2)$ in Ω referred as *the equilibrium vector field*. Its singular points describe the pure components and the azeotropes of a given mixture. That is, *the singular points of the RCM*. Below we use the symbol "∧" for the wedge product of two vectors on the plane:

$$\bar{x} \wedge \bar{v} = v_2 x_1 - v_1 x_2 = det \begin{bmatrix} x_1 & x_2 \\ v_1 & v_2 \end{bmatrix}$$

It is easy to see that the wedge product of two vectors is zero if and only if either at least one of them is a zero vector, or the two vectors are collinear, i.e. $\bar{v} = a\bar{x}$ for some scalar $a \neq 0$.

The *relative volatility* of component i with respect to component j is given by the ratio

$$\alpha_{ij} = \frac{y_i/x_i}{y_j/x_j} = \frac{K_i}{K_j}$$

If $\alpha_{ij} > 1$, i is more volatile than j and vice versa. The *univolatility curves* are the sets of points in Ω satisfying $\alpha_{ij} = 1$. The RCM of a given ternary mixture may contain up to 3 types of α-curves defined by their respective indices i, j. Geometrically, these curves are formed by the intersections of the boiling temperature surface, W, with one of the *univolatility hypersurfaces* defined by equations in the form

$$\Psi_{ij}(\bar{x}, T) = K_i(\bar{x}, T) - K_j(\bar{x}, T) = 0 \qquad (4)$$

We will call the solutions to Eqs. (1) and (4), the *generalized univolatility curves*. The univolatility curves are the projections of the generalized univolatility curves on the (x_1, x_2) -plane, satisfying for the relevant pair i-j

$$\psi_{ij}(\bar{x}, T_b(\bar{x})) = K_i(\bar{x}, T_b(\bar{x})) - K_j(\bar{x}, T_b(\bar{x})) = k_i(\bar{x}) - k_j(\bar{x}) = 0 \qquad (5)$$

Here $k_i(\bar{x}) = K_i(\bar{x}, T_b(\bar{x}))$ denotes the restriction of the i-th distribution coefficient to the boiling temperature surface, W. In what follows we will systematically use uppercase letters for the objects defined in the three-dimensional state space, and lowercase for the corresponding projections on Ω.

Fig. 1 shows the ternary vapor – liquid equilibrium for the mixture acetone (x_1) – ethyl acetate (x_2) – benzene. This mixture forms no azeotropes. One univolatility curve, $\alpha_{2,3} = 1$, between ethyl acetate and benzene exists linking the binary edges acetone – ethyl acetate and acetone – benzene. Fig. 1 also shows the mutual arrangement of the boiling temperature surface W and the univolatility hypersurface Ψ_{23} for this zeotropic ternary mixture. The curve Θ formed by their intersection is the generalized univolatility curve. Its projection (full curve) on the triangular diagram, Ω, is the univolatility curve, here of type $\overline{\overline{\alpha_{2,3}}}$, satisfying the thermodynamic condition, $\psi_{23}(\bar{x}, T_b(\bar{x})) = 0$. The shape and the location of univolatility hyper-surfaces are independent of pressure, when the vapor phase is an ideal gas. In contrast, the boiling temperature surface W moves up in the three dimensional state space when pressure increases. Its shape can also change. Such a transformation of W can be traced out by considering the transformation of the underlying RCM with pressure variation, as we show in Section 3. The described geometrical picture is essentially related to the ternary mixtures. Indeed, in the higher dimensional case the relation $\alpha_{ij} = 1$ describes hypersurfaces in the composition space Ω instead of curves. Consequently, the computation method presented below is only valid for ternary mixtures.

The structure of the univolatility curves is closely related to the structure of the unidistribution curves (Kiva et al., 2003), that is the curves in Ω along which $k_i = 1$ for i = 1, 2, 3. In Fig. 1 these curves are represented by dashes. An unidistribution curve is a projection on Ω of the intersection of the boiling temperature surface, W, with a unidistribution hypersurface defined by $K_i(x_1, x_2, T) = 1$.
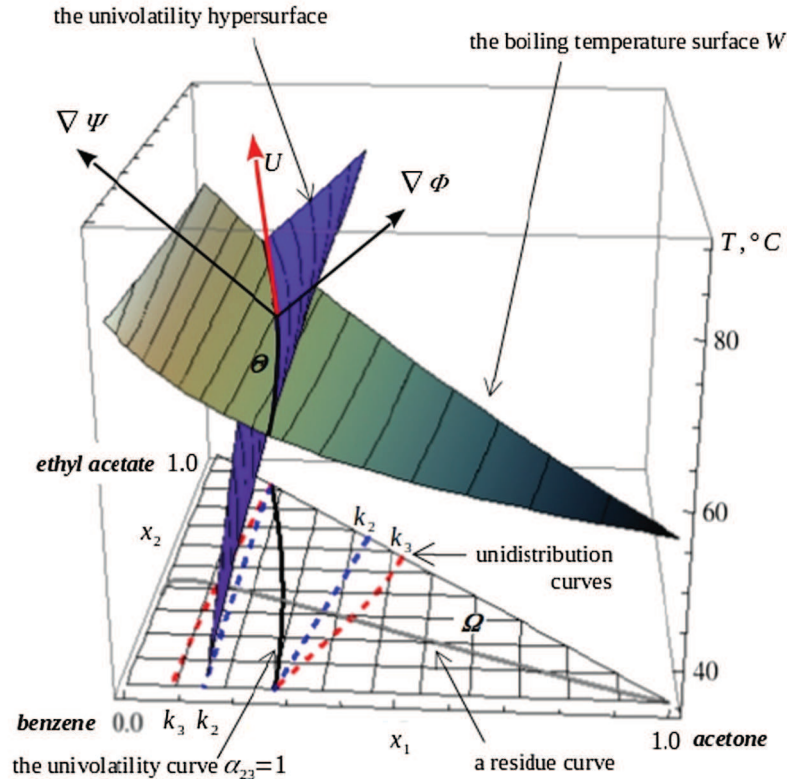
Fig. 1. Boiling temperature surface W and the univolatility hypersurface $\Psi_{23} = 0$ where $\alpha_{23} = 1$ for the mixture acetone (1) – ethyl acetate (2) – benzene (3).

2.2. Unidistribution and univolatility curves in the composition space

2.2.1. The role of distribution coefficients in detecting the existence of the unidistribution and the univolatility curves

If the binary side i-j of the composition triangle Ω contains a binary azeotrope, then at this point $k_i = k_j = 1$. Hence this point belongs to the intersection of a pair of unidistribution curves and to the univolatility curve $\alpha_{ij} = 1$. Kiva et al. (2003) highlighted the relationship between distribution coefficient functions $k_i(\bar{x})$ of each binary pair, with the presence of unidistribution and the univolatlity curves, using the concept of the *distribution coefficient at infinite dilution*. More precisely $k_m^{\infty ij} = \lim_{x_{m-0}} k_m$ for $m \neq i, j$. We can compute three functions $k_m^{\infty ij}$, k_i^{ij}, and k_j^{ij} for each binary i-j. The last two are the distribution coefficients of the binary system formed by components i and j. Below we use the term *distribution curve* for the graphs of these functions along binary i-j side of the composition triangle. If, at such a point, both distribution coefficients k_i^{ij}, and k_j^{ij} are unity, the point is a binary azeotrope (denoted Az_{ij}) of the mixture "i,j". On the other hand, the binary composition corresponding to the intersection point of a pair of distribution curves $k_m^{\infty ij}$ and k_i^{ij} (or k_j^{ij}) yields the starting point of the univolatility curve $\alpha_{i,m} = 1$ (or $\alpha_{j,m} = 1$). Similarly, if at some composition of the binary i-j the function $k_m^{\infty ij}$ is unity, this composition initiates the unidistribution curve of component m.

Fig. 2 illustrates these concepts for the ternary mixture acetone (1) – chloroform (2) – methanol (3), including the functions $k_m^{\infty ij}$, k_i^{ij}, and k_j^{ij} and the univolatility and unidistribution curves.

As shown in Fig. 2, each binary pair has a single azeotrope, and there is one ternary azeotrope (saddle type). Each univolatility curve α_{ij} beginning at the binary i-j azeotrope terminates at the binary composition corresponding to the intersection of either

$(k_i^{\infty m,j}, k_j^{m,j})$ or $(k_i^{\infty i,m}, k_i^{i,m})$. In particular, the curve $\alpha_{1,2} = 1$ reaches the edge *1–3* at the intersection of $k_2^{\infty 1,3}$ and $k_1^{1,3}$. The curve $\alpha_{1,3} = 1$ reaches the edge *2–3* at the intersection of $k_1^{\infty 2,3}$ and $k_3^{2,3}$. Similarly, the curve $\alpha_{2,3} = 1$ reaches the edge *1–3* at the intersection of $k_2^{\infty 1,3}$ and $k_3^{1,3}$. Thus, all starting points of univolatility and unidistribution curves can be determined by the computation of the distribution coefficients $k_i(\bar{x})$ in the binaries only. Next, we will focus on the thermodynamic interpretation of the univolatility curves.

2.2.2. Thermodynamic meaning of the unidistribution and the univolatility curve

Consider a residue curve $\beta(\xi) = (x_1(\xi), x_2(\xi))$ in Ω and the univolatility curve $\alpha_{1,2} = 1$. By definition, β is a solution to the differential equation $\dot{\bar{x}} = \bar{v}$. Moreover, along β the following relations holds

$$(k_1 - k_2)|_{\bar{x} \in \beta(\xi)} = \frac{y_1 x_2 - y_2 x_1}{x_1 x_2} = \frac{\bar{x} \wedge \bar{v}}{x_1 x_2} = \frac{\dot{x}_2 x_1 - \dot{x}_1 x_2}{x_1 x_2}$$

$$= \frac{d}{d\xi}\left(\ln \frac{x_2}{x_1}\right) \tag{6}$$

$$\frac{d}{d\xi}(k_1 - k_2)|_{\bar{x} \in \beta(\xi)} = \frac{\bar{x} \wedge \ddot{\bar{x}}}{x_1 x_2} - (k_1 - k_2)\frac{x_1 v_2 + x_2 v_1}{x_1 x_2} \tag{7}$$

The detailed derivation of equalities (6) and (7) is given in Appendix A.

Suppose the curve β intersects the univolatility curve $\alpha_{1,2} = 1$ at some point $\bar{x}_* = \beta(\xi_*)$. Then $k_1(\bar{x}_*) - k_2(\bar{x}_*) = 0$ and at the point $\bar{x}_*$ the left-hand side of Eq. (6) vanishes. Since the natural logarithm is a monotonous function, this implies that $\bar{x}_*$ is the critical point of the ratio x_2/x_1 along β. In particular, $\bar{x}_*$ satisfies the necessary
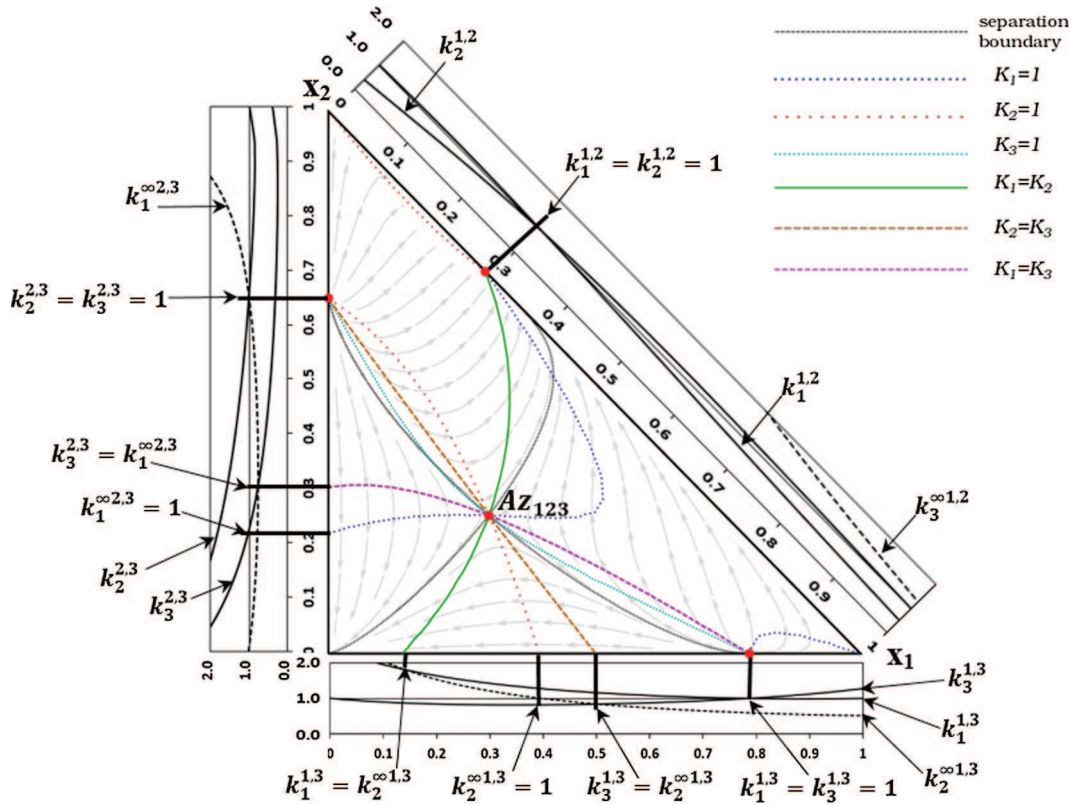
Fig. 2. Relationship between univolatility curves and distribution curves for the mixture acetone (1) – chloroform (2) – methanol (3).

conditions for the solutions of the constrained optimization problem on the form

$$\min/\max_{\bar{x}(\xi)\in\beta} \frac{x_2(\xi)}{x_1(\xi)}$$

Geometrically, this means that the slope of the ray issued from the origin and moving along the residue curve β has an extremum at the point where the residue curve intersects the univolatility curve $\alpha_{1,2} = 1$. Since $(k_1 - k_2)(\overline{x_*}) = 0$, only the wedge product term remains in Eq. (7). It follows that the function $x_2(\xi)/x_1(\xi)$ has a local maximum at ξ_* if $\bar{x}_* \wedge \ddot{\bar{x}}(\xi_*) < 0$ and a local minimum if $\bar{x}_* \wedge \ddot{\bar{x}}(\xi_*) > 0$, except at an inflection point where $\bar{x}_* \wedge \ddot{\bar{x}}(\xi_*) = 0$. In the latter case ξ_* corresponds to the inflection point of the ratio $x_2(\xi)/x_1(\xi)$.

Recall that the curvature of a curve on a plane is given by $\chi = \dot{\bar{x}} \wedge \frac{\ddot{\bar{x}}}{||\dot{\bar{x}}||^3}$ (Do Carmo, 1976). Comparing Eq. (6) with residue curves of Eqs. (3) we see that at the point $\bar{x}_*$ the vectors $\bar{x}$ and $\bar{v} = \dot{\bar{x}}$ are collinear, so the type of the extremum is defined by the sign of the curvature χ. The sign of the curvature characterizes the convexity of the curve. Indeed, when $\dot{x}_1 \neq 0$, the curve β can be represented as a graph of the form $x_2 = x_2(x_1)$. In this case $\chi = x_2''(1 + (x_2')^2)^{-3/2}$, where "$\prime$" denotes the derivative with respect to x_1, and hence $\chi > 0$ corresponds to convex curves, while $\chi < 0$ corresponds to concave curves. Moreover, residue curves Eq. (3) imply that at the point of intersection with the univolatility curve $x_2' = \frac{x_2}{x_1} \geqslant 0$. This means that residue curves intersect the univolatility curve $\alpha_{1,2} = 1$ in the ascending direction (with respect to the chosen pair of axes). All of this remains true for the univolatility curves $\alpha_{1,3} = 1$ and $\alpha_{2,3} = 1$ modulo the initial choice of the coordinate axes. Putting together these arguments, we get the following results:

Theorem 1.

(a) *Univolatility curves $\alpha_{i,j}$ on the RCM of ternary mixtures are the loci of the critical points of the relative compositions x_j/x_i.*

(b) *Along any residue curve, the type of the local extremum of the ratio x_j/x_i at the point of the intersection with the univolatility curve $\alpha_{i,j} = 1$ is determined by the sign of its curvature at this point, with respect to the axes x_i, x_j: It has a minimum if $\chi > 0$, and a maximum if $\chi < 0$.*

(c) *Any residue curve intersecting the univolatility curve $\alpha_{i,j} = 1$ at the point $\bar{x}_*$ is tangent to the ray $x_{*j}/x_{*i} = const$. It intersects the univolatility curve in ascending direction with respect to the axes x_i, x_j. Moreover, if the curvature of this residue curve has constant sign, the whole curve will entirely lie on the same side of the ray $x_{*j}/x_{*i} = const$.*

Remark 1. The geometrical characterization given in property **c** is well known in the literature (Kiva et al. 2003).

Remark 2. Azeotropes and pure states are singular points for the equilibrium vector field, v. Hence, they are asymptotic limits of the residue curves, as ξ goes to infinity in Eq. (3). In other words, residue curves do not pass through them. Consequently, azeotropes and pure states are excluded from the context of Theorem 1. In order to detect the global extremum value of the relative composition along a residue curve, one has to consider the asymptotic upper and lower limits associated to straight curves $x_i/x_j = const$ connecting the pure states to the azeotropes associated with the residue curve under consideration.

The ternary mixture of acetone (1) – chloroform (2) – methanol (3) (shown in Fig. 2), has one ternary azeotrope of saddle type and 3 binary azeotropes as nodes. In Fig. 3 we present the sketch of its
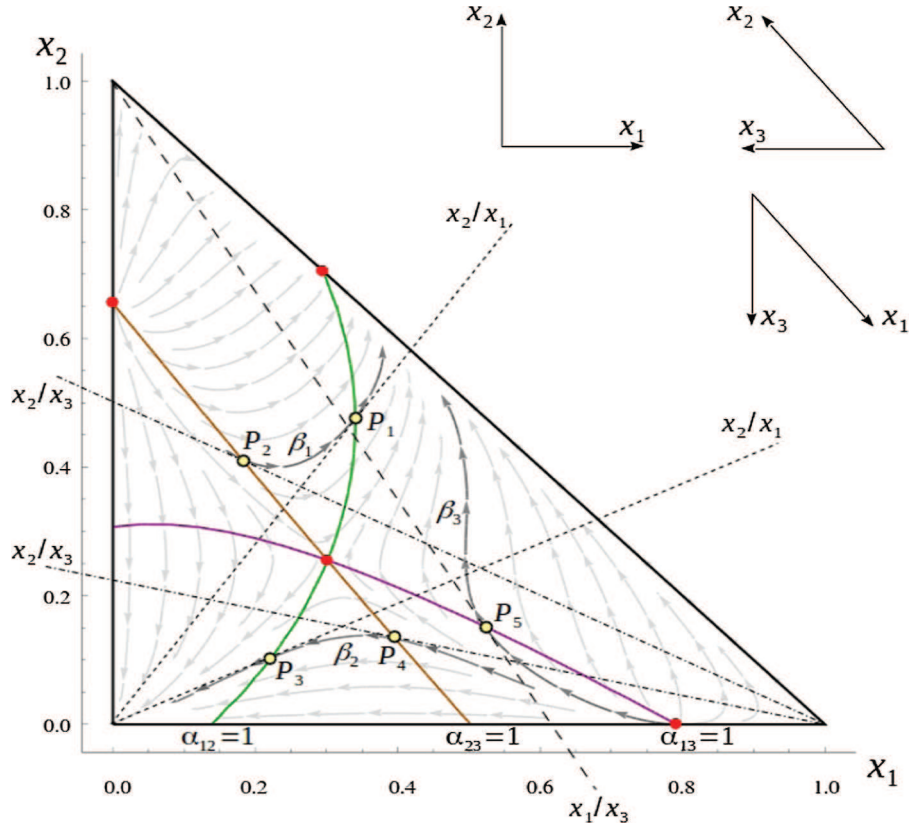
Fig. 3. Relationship between univolatility curves and residue curves for the mixture acetone (1) – chloroform (2) – methanol (3).

RCM. For the sake of convenience, in the upper right corner we recall the orientation of the axes for the coordinate systems having the origin at different pure states. Azeotropes are indicated by red dots. The three full curves are univolatility curves. Consider first the residue curve β_1. Along this curve the ratio x_2/x_1 has a local minimum at the point P_1 where it intersects the univolatility curve $\alpha_{1,2} = 1$, and at P_2 (intersection with $\alpha_{2,3} = 1$) the local mimimum value of x_2/x_3 is reached. Along the curve β_2 the function x_2/x_1 has a local maximum at P_3 (intersection with $\alpha_{1,2} = 1$) and at P_4, x_2/x_3 has local maximum (intersection with $\alpha_{2,3} = 1$). Finally, along β_3 there is a local minimum of x_1/x_3 at the point P_5 (intersection with $\alpha_{1,3} = 1$).

2.3. Practical computation of the unidistribution and univolatility curves

2.3.1. Detection of the starting points of the unidistribution and the univolatility curves on the binary sides of the composition space Ω

As shown in Fig. 1, the existence of the univolatility curves can be detected from the equality of the values of the binary distribution coefficients, including the coefficients of the components at infinite dilution. The formal calculation of the starting points of the univolatility curves relies upon the solution of the algebraic equations (5) restricted to the binary mixtures. Such a restriction means that the k_i must be replaced by the appropriate binary distribution coefficients or the distribution coefficient at infinite dilution. Eq. (5) describing the univolatility curves are restrictions of Eq. (4) to the boiling temperature surface defined by Eq. (1). Since along the binary side i-j, we have $x_i = 1 - x_j$ and $x_m = 0$, this side can be parametrized by a single composition variable x_j. Thus, for any binary i-j we have to solve the following system of algebraic equations:

$$K_i^{i,j}(x_j, T) - K_j^{i,j}(x_j, T) = 0, \quad K_i^{i,j}(x_j, T)(1 - x_j) + K_j^{i,j}(x_j, T)x_j = 1$$
(8.1)

$$K_i^{i,j}(x_j, T) - K_m^{\infty i,j}(x_j, T) = 0, \quad K_i^{i,j}(x_j, T)(1 - x_j) + K_j^{i,j}(x_j, T)x_j = 1$$
(8.2)

$$K_j^{i,j}(x_j, T) - K_m^{\infty i,j}(x_j, T) = 0, \quad K_i^{i,j}(x_j, T)(1 - x_j) + K_j^{i,j}(x_j, T)x_j = 1$$
(8.3)

Here, as before, $K_m^{\infty i,j} = \lim_{x_{m \to 0}} K_m$. Thermodynamic models are needed for the pure component vapor pressures and the activity coefficients of all 3 species i-j-m.

Computation of starting points for the unidistribution curves is completely analogous. But, the first equation in each of the systems (8.1)–(8.3) must be replaced by one of the following equations,

$$K_i^{i,j}(x_j, T) = 1, K_j^{i,j}(x_j, T) = 1, \ K_m^{\infty i,j}(x_j, T) = 1$$
(9)

The algorithm of the computation of the starting points of the unidistribution and univolatility curves, using Eqs. (8.3) or (9) does not require the existence of binary azeotropes. It is applicable to any zeotropic or azeotropic homogeneous mixture. However, all binary azeotropes, if they exist, will be found as solutions. In the next section we will derive the ordinary differential equation allowing computation of the whole univolatility or unidistribution curve by numerical integration.

2.3.2. The generalized univolatility and unidistribution curves

Consider a generalized univolatility curve $\Theta : \tau \rightarrow \Theta(\tau) = (x_1(\tau), x_2(\tau), T(\tau))$ in the three-dimensional state space. By definition, Θ is formed by the intersection of two hypersurfaces defined by the algebraic equations $\Phi(x_1, x_2, T) = 0$, $\Psi(x_1, x_2, T) = 0$, the

latter representing any of the Eqs. (4). A short recall about surface geometry is given in Appendix B.

Let $U = (U_1, U_2, U_3)$ denote a tangent vector to Θ at some point. By construction, U is orthogonal both to the normal vector $N_w = \nabla\Phi$ to the boiling temperature surface W and to the normal $N = \nabla\Psi$ to the univolatility hypersurface (see Fig. 1). If the two hyper-surfaces are in general position (i.e. do not have common tangent planes), we have $U = N_w \times N$, implying

$$U_1 = \frac{\partial\Phi}{\partial x_2}\frac{\partial\Psi}{\partial T} - \frac{\partial\Phi}{\partial T}\frac{\partial\Psi}{\partial x_2}, \quad U_2 = \frac{\partial\Phi}{\partial T}\frac{\partial\Psi}{\partial x_1} - \frac{\partial\Phi}{\partial x_1}\frac{\partial\Psi}{\partial T},$$
$$U_3 = \frac{\partial\Phi}{\partial x_1}\frac{\partial\Psi}{\partial x_2} - \frac{\partial\Phi}{\partial x_2}\frac{\partial\Psi}{\partial x_1} \tag{10}$$

Theorem 2. *The generalized univolatility curve projecting on the univolatility curve $\alpha_{ij} = 1$ is an integral curve of the vector field U defined by Eq. (10), i.e., it is a solution to the following system of ordinary differential equations in three-dimensional state space:*

$$\frac{dx_1}{d\tau} = \frac{\partial\Phi}{\partial x_2}\frac{\partial\Psi_{ij}}{\partial T} - \frac{\partial\Phi}{\partial T}\frac{\partial\Psi_{ij}}{\partial x_2}, \quad \frac{dx_2}{d\tau} = \frac{\partial\Phi}{\partial T}\frac{\partial\Psi_{ij}}{\partial x_1} - \frac{\partial\Phi}{\partial x_1}\frac{\partial\Psi_{ij}}{\partial T},$$
$$\frac{dT}{d\tau} = \frac{\partial\Phi}{\partial x_1}\frac{\partial\Psi_{ij}}{\partial x_2} - \frac{\partial\Phi}{\partial x_2}\frac{\partial\Psi_{ij}}{\partial x_1} \tag{11}$$

The geometrical interpretation of Theorem 2 is illustrated in Fig. 1.

Remark 3. In principle, the boiling temperature surface and the univolatility hypersurface can have isolated points of common tangency. In this case $U_1 = U_2 = U_3 = 0$, i.e., the generalized univolatility curve degenerates into a point. Comparing Eqs. (11) and (2), after all necessary simplifications, gives

$$U_3 = U_1\frac{\partial T_b}{\partial x_1} + U_2\frac{\partial T_b}{\partial x_2}, \tag{12}$$

and therefore any singular point of the univolatility curve on Ω obeying $U_1 = U_2 = 0$ is a singular point of the corresponding generalized univolatility curve and vice versa. Such isolated singular points can be of elliptic or hyperbolic type. In the first case the corresponding degenerated univolatility curve will just be a point in Ω, whereas in the last case it is composed of four branches joining at the singular point. Note that such singular points of univolatility curves are not necessarily singular points of the RCM. Another highly non-generic situation occurs when a curve of $\overline{\alpha_{ij}}$ type shrinks into a point on the binary edge of the composition space Ω. Such point can be either a regular point of the RCM or it can coincide with a tangential binary azeotrope. In the latter case the RCM will have a binary azeotrope which does not generate any univolatility curve that is different from a point. In Section 3 we provide the examples of these highly non-generic and unusual configurations.

Remark 4. All the above formulae can be directly applied for the computation of the unidistribution curves by setting $\Psi(x_1, x_2, T) = K(x_1, x_2, T) - 1$, where K is any of the distribution coefficients.

2.3.3. From three-dimensional model to the numerical computation of the univolatility curves

Eq. (11) provides an effective tool for numerical computation of the univolatility curves using the standard Runge-Kutta schemes for the ODE integration. The initial points for such integration can be computed by finding solutions of Eqs. (8.1)–(8.3) by means of a standard non-linear equations solver like the Newton-Raphson method. Once the initial point is chosen, the whole generalized univolatility curve can be computed by following the intersection of two associated hyper-surfaces using the vector field U in the direction pointing inside the composition space Ω. In particular, no further iteration procedure is required to compute the univolatility curve in the interior points of Ω. In addition, to avoid the difficulties associated with possible stiffness of Eqs. (11), it is recommended to rewrite them in the normalized form, which is equivalent to choose the arc length s of the curve as the new parameter of integration instead of τ.

For definiteness, consider the curve $\alpha_{i,j} = 1$ starting from the *3–1* binary side, that is, from the x_1-axis. The starting point of this curve is a projection of a point $(x^0_{1,ij}, 0, T^0_{1,ij})$ in the state space. The whole curve $\alpha_{i,j} = 1$ can be computed as the projection of the solution of the following initial value problem:

$$\frac{dx_1}{ds} = \frac{d_{ij}U^{ij}_1(x_1, x_2, T)}{\|U^{ij}(x_1, x_2, T)\|}, \quad \frac{dx_2}{ds} = \frac{d_{ij}U^{ij}_2(x_1, x_2, T)}{\|U^{ij}(x_1, x_2, T)\|},$$
$$\frac{dT}{ds} = \frac{d_{ij}U^{ij}_3(x_1, x_2, T)}{\|U^{ij}(x_1, x_2, T)\|} \tag{13}$$

$$x_1(0) = x^0_{1,ij}, \quad x_2(0) = 0, \quad T(0) = T^0_{1,ij} \tag{14}$$

$$d_{ij} = sign\left(U^{ij}_2\left(x^0_{1,ij}, 0, T^0_{1,ij}\right)\right) \tag{15}$$

Analogous initial value problems can be formulated for the curves starting from other binary sides of Ω by an appropriate modification of the initial conditions (14) and the starting direction (15). Here is the sketch of the general algorithm:

1. Find all starting points of the univolatility curves on each binary side *i-j* of Ω and form the list of all possible starting points by solving Eqs. (8.1)–(8.3).
2. Take the starting points of the list created in point 1 and solve the initial value problem of type (13)–(15) with an appropriate choice of the initial direction. The numerical integration should be continued until one of the following situations occurs: $x_1 < 0, x_2\langle 0, x_1 + x_2\rangle 1$, i.e. the border of Ω is attained. Then stop integration.
3. Exclude both initial and final points of the curve computed in point 2 from the list of starting points.
4. Go back to point 2 until the list of starting points is exhausted.

The advantage of the described algorithm is that once the Eq. (13) is given, we only need to use a standard solver for a pair of non-linear algebraic equations and a standard ODE integrator. The prototype of the algorithm described above was realized in Mathematica 9, and was used in case studies discussed in the next section. The choice of Mathematica 9 is not prohibitive. The algorithm can easily be implemented in other scientific computing packages like MATLAB of MAPLE allowing Eq. (13) to be written by symbolic differentiation of the thermodynamic model. The implementation using the standard algorithmic languages is possible by coupling with a compatible library of automatic differentiation.

Remark 5. The above method of calculation of the univolatility and unidistribution curves was developed under the ideality assumption of the vapor phase. Although the geometrical derivation remains the same, certain definitions and computations must be adapted when considering a non-ideal vapor phase. In that case, and in order to correctly define the concept of the univolatility curve in the composition space Ω, the relations $y_i = K_i(\overline{x}, \overline{y}, T)x_i$,

$i = 1, 2, 3$, need first to be solved with respect to the vapor mole fractions y_i. In principle, this is possible thanks to the general Implicit Function Theorem, which also provides the explicit formulae for the derivatives of y_i with respect to x_i and T. In the presented numerical algorithm, a standard ODE solver needs to be replaced by a DAE solver, allowing to compute the vapor phase at each step of integration.

3. Computation of univolatility curves in ternary mixtures. Case studies

Reshetov and Kravchenko (2007a, 2007b) studied 6400 ternary mixtures including 1350 zeotropic mixtures, corresponding to Serafimov class 0.0–1. The structure of the univolatility curves was determined for 788 zeotropic systems, using the Wilson activity coefficient equation based on both, ternary experimental data and reconstructed data of binary mixtures. 15 of the possible 33 classes defined by Zhvanetskii et al. (1988) were found, and 28.4% of computed ternary diagrams exhibited at least one univolatility curve indicating the necessity of computing the univolatility curve even for zeotropic mixtures. Unfortunately, the authors provided no information on the components used in their analysis. In the case of ternary mixtures with at least one azeotrope, Reshetov and Kravchenko (2010) extended their earlier study (Reshetov et al. 1990) by considering 5657 ternary mixtures where 30% of all cases were modelled from experimental data. Table 1 summarizes Reshetov and Kravchenko results (2010) and arranges ternary diagrams into three groups according to the number of $\alpha_{i,j}$ curves of each component pair "i,j". We use Serafimov's classification instead of Zharov's classification (see correspondence in Kiva et al., 2003) used in the original paper. According to Table 1, 79.2% of the analysed mixtures had at least one univolatility curve. Among them, 97.2% have only one univolatility curve $\alpha_{i,j}$ for each index "i,j", while 2.7% involved two univolatility curves $\alpha_{i,j}$. Two ternary diagrams belonging to the Serafimov class (1.0-1a) exhibited three univolatility curves $\alpha_{i,j}$ with the same component index "i,j". Furthermore, about 2% of studied cases displayed at least one univolatility curve of $\overline{\alpha_{i,j}}$ -type. According to these data, real ternary mixtures exhibiting more than one univolatility curve for a component index "i,j", as well as the $\overline{\alpha_{i,j}}$-type univolatility curve are rare at atmospheric pressure. Below we present two

examples with quite an uncommon behavior related to the existence of at least two univolatility curves with the same component index "i,j" and one univolatility curve belonging to $\overline{\alpha_{i,j}}$ -type. The first example is the ternary mixture diethylamine (1) – chloroform (2) – methanol (3) which was reported in the paper of Reshetov and Kravchenko (2010) as exhibiting two univolatility curves $\overline{\overline{\alpha_{1,2}}}$. The second example is the well-known case of the existence of two binary azeotropic mixture for benzene – hexafluorobenzene providing a particular shape of the univolatility curves. The atmospheric pressure was selected for defining the initial Serafimov class of the RCM for each case study. The RCMs were computed using NRTL model with Aspen Plus built-in binary interaction parameters. For the binary mixture diethylamine (1) – chloroform (2), the binary coefficients were determined from experimental vapor – liquid equilibrium data (Jordan et al., 1985).

3.1. Case Study: diethylamine (1) – chloroform (2) – methanol (3)

In Fig. 4 we show the RCM of this mixture at 1 atm. It has two binary maximum boiling azeotropic points in the binary edges diethylamine (1) – chloroform (2) and diethylamine (2) – methanol (3), and one binary minimum boiling azeotrope on the edge chloroform (2) – methanol (3). The corresponding Serafimov class is 3.0-1b with only 0.9% of occurrence (Hilmen et al., 2002). At 1 atm, there are three univolatility curves of $\overline{\alpha_{i,j}}$-type coming from each binary azeotrope. This is consistent with the behavior of the distribution curves along the binary sides *1–2*, *1–3* and *2–3* (right diagrams) and the unity level line. The univolatility curve $\alpha_{1,3} = 1$ issued from Az_{13} arrives at the edge *1–2* at the intersection point of the curves $k_3^{\infty 1,2}$ and $k_1^{1,2}$. Similarly, the curve $\alpha_{1,2} = 1$ starts at Az_{12} and reaches the edge *1–3* at the point corresponding to the intersection of the distribution curves $k_2^{\infty 1,3}$ and $k_1^{1,3}$, and the curve $\alpha_{2,3} = 1$ issued from Az_{23} terminates at the point given by the intersection of the curves $k_2^{\infty 1,3}$ and $k_3^{1,3}$. As a consequence of the difference in nature of the azeotropes and the close boiling temperatures of the components, diethylamine (55.5 °C) – chloroform (61.2 °C) – methanol (64.7 °C), the small variation of the pressure causes a significant transformation of the topological structure of the univolatility curves.

Indeed, as it is shown in Fig. 5, changing the pressure to 0.5 atm leads to several bifurcations of the topological structure of RCM

Table 1
Occurrence of univolatility curves having different types in several Serafimov classes of ternary diagrams according to []. adapted from Reshetov and Kravchenko, 2010

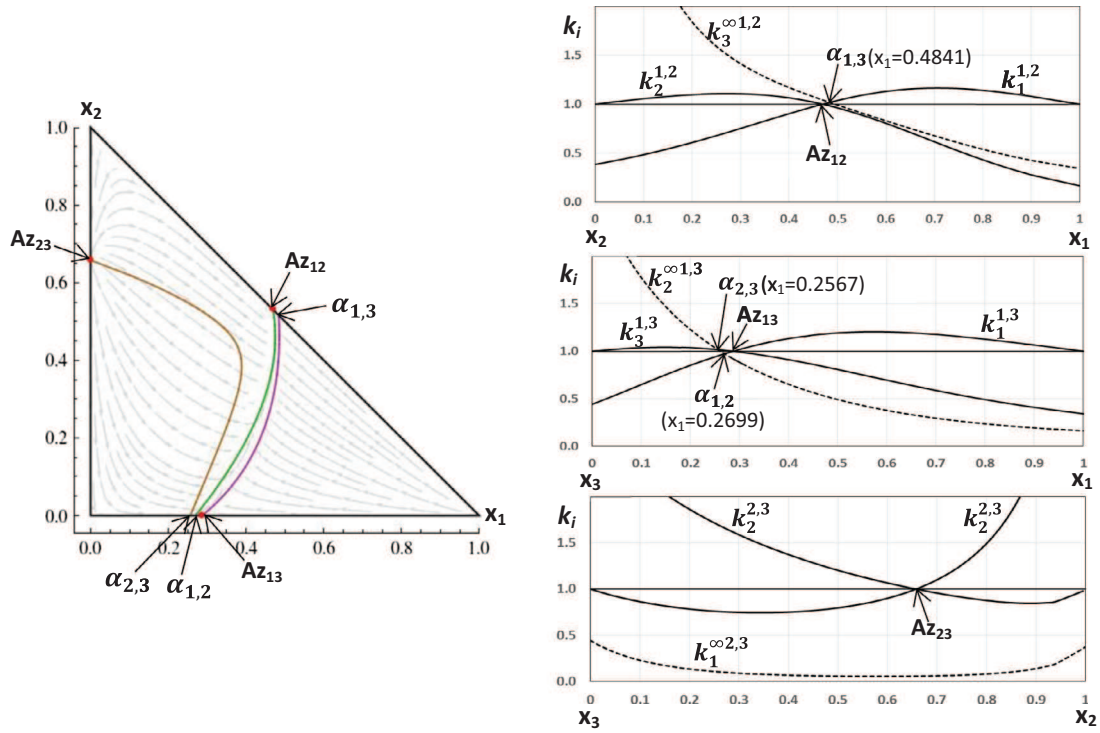| Serafimov's class	One $\alpha_{i,j}$		Two $\alpha_{i,j}$		Three $\alpha_{i,j}$	
	$\overline{\alpha_{i,j}}$	$\overline{\overline{\alpha_{i,j}}}$	$\overline{\alpha_{i,j}}$	$\overline{\overline{\alpha_{i,j}}}$	$\overline{\alpha_{i,j}}$	$\overline{\overline{\alpha_{i,j}}}$
1.0-1a[*]	1	938	11	29	–	2
1.0-1b[*]	–	49	1	–	–	–
1.0-2[*]	19	682	5	15	–	–
2.0-1	–	23	–	–	–	–
2.0-2a[*]	–	3	–	2	–	–
2.0-2b[*]	14	1975	3	24	–	–
2.0-2c	–	63	–	1	–	–
3.0-2	–	174	–	10	–	–
3.0-1b[*]	–	29	1	2	–	–
1.1-2	7	27	5	0	–	–
1.1-1a	1	–	–	–	–	–
2.1-2b	5	32	–	1	–	–
2.1-3b[*]	10	59	2	5	–	–
2.1-3a	–	29	–	–	–	–
3.1-2	–	168	–	5	–	–
3.1-1b	–	2	–	–	–	–
3.1-1a	–	2	–	–	–	–
3.1-4[*]	–	47	–	–	–	–

[*] Antipodal structure.

Fig. 4. RCM, univolatility curves and distribution curves on the edges 1–2, 1–3 and 2–3 for the mixture diethylamine (1) – chloroform (2) – methanol (3) at P = 1 atm.

along with the transformation of the structure of both univolatility and distribution curves. First, the pressure is slightly decreased (Fig. 5a) and a new branch of $\overline{\overline{\alpha_{2,3}}}$ type arises from the edge diethylamine (1) – chloroform (2). This new branch is not connected to any azeotropic point. With further pressure decrease, the two univolatility curves $\overline{\alpha_{2,3}}$ and $\overline{\overline{\alpha_{2,3}}}$ get closer until the first bifurcation appearing at P $\approx$ 0.922148 atm (see Fig. 5b): the two branches of the curve $\alpha_{2,3} = 1$ meet each other at a singular point. Such a singularity resulting from the common tangency between the boiling temperature surface and the univolatility hypersurface was described in Remark 3 in the Section 2.3.2. In the present case the situation is even more interesting because at this singular point the curve $\alpha_{2,3} = 1$ intersects the other two univolatility curves forming a ternary azeotrope Az_{123} of the saddle-node type. With decreasing pressure slightly (Fig. 5c) the saddle–node azeotrope splits into a pair of ternary azeotropes: a saddle (the upper one) and a stable node (the lower one). The curve $\alpha_{2,3} = 1$ is now formed by two branches of $\overline{\overline{\alpha_{2,3}}}$ type.

With a further decrease of pressure (Fig. 5d) the saddle ternary azeotrope merges with the binary azeotrope diethylamine (1) – chloroform (2) at P $\approx$ 0.90212323 atm, forming a transient tangential binary azeotrope. An infinitesimal reduction of the pressure gives rise to a binary azeotrope Az_{12} of saddle type. The resulting RCM corresponds to the Serafimov class 3.1-1b which has zero occurrence in real mixtures according to Hilmen et al. (2002).

The next bifurcation occurs at P $\approx$ 0.7574595 atm (Fig. 5e): the three univolatility curves $\alpha_{i,j} = 1$ meet each other on the binary side diethylamine (1) – methanol (3) forming a tangential binary azeotrope Az_{13}. Continued pressure reduction (Fig. 5f) moves the bottom of the curve $\alpha_{2,3} = 1$ to the right inducing the splitting of the transient azeotrope into a binary stable node and a new ternary azeotrope of saddle type. We observe again a RCM with 2 ternary azeotropes in Fig. 5f: a saddle (in the bottom) and a stable node (in the top) resulting from the double intersection of the three univolatility curves of different types. At P $\approx$ 0.627963 atm (Fig. 5g),

two ternary azeotropes merge in a single saddle-node ternary azeotrope, which disappears with a further pressure decrease. Below this singular value of pressure and until P = 0.5 atm, the RCM belongs again to Serafimov class 3.0-1b as it was at P = 1 atm. However, the maximum boiling azeotropic mixture diethylamine (1) – methanol (3) is now the stable node type instead of the mixture diethylamine (1) – chloroform (2) at P = 1 atm (Fig. 4). Note, that the resulting two RCMs of Serafimov class 3.0-1b have different topology of univolatility curves. At 0.5 atm there is one curve of type $\overline{\alpha_{1,3}}$, one curve of type $\overline{\alpha_{1,2}}$ and two curves of type $\overline{\alpha_{2,3}}$ instead of just one curve of type $\overline{\alpha_{i,j}}$ for each pair of indices.

Comparing the RCM diagrams in Fig. 5 to the corresponding distribution curves in Fig. 6, shows that the bifurcation resulting from the intersection of more than one univolatility curves at the binary edges can be detected by the analysis of the intersections of the distribution curves associated with the distribution coefficients $k_m^{\infty i,j}$, $k_i^{i,j}$ and $k_j^{i,j}$. Indeed, in Fig. 6a-c and Fig. 6f, both terminal points of the curve $\overline{\overline{\alpha_{2,3}}} = 1$ with the binary side diethylamine (1) – chloroform (2) correspond to the double intersection of the distribution curves of $k_3^{\infty 1,2}$ and $k_2^{1,2}$. These results show the efficiency of this criterion for the curves of type $\overline{\alpha_{i,j}}$. In Fig. 6d the existence of the tangential binary azeotrope Az_{12} on the 1–2 edge is well in accordance with the common intersection point of the three distribution curves $k_3^{\infty 1,2}$, $k_1^{1,2}$ and $k_2^{1,2}$. The same behavior can be also observed by comparing Figs. 5e and 6e for the binary tangential azeotrope on the edge diethylamine (1) – methanol (3): the three distribution curves $k_2^{\infty 1,3}$, $k_1^{1,3}$ and $k_3^{1,3}$ intersect at the azeotropic composition Az_{13}. The formation (Fig. 5b and g) and the splitting (Fig. 5c and f) of the saddle-node type ternary azeotropes cannot be detected from the behavior of the distribution curves along binary edges. The existence of the ternary azeotropes is detected by the existence of the intersection of at least two univolatility curves.
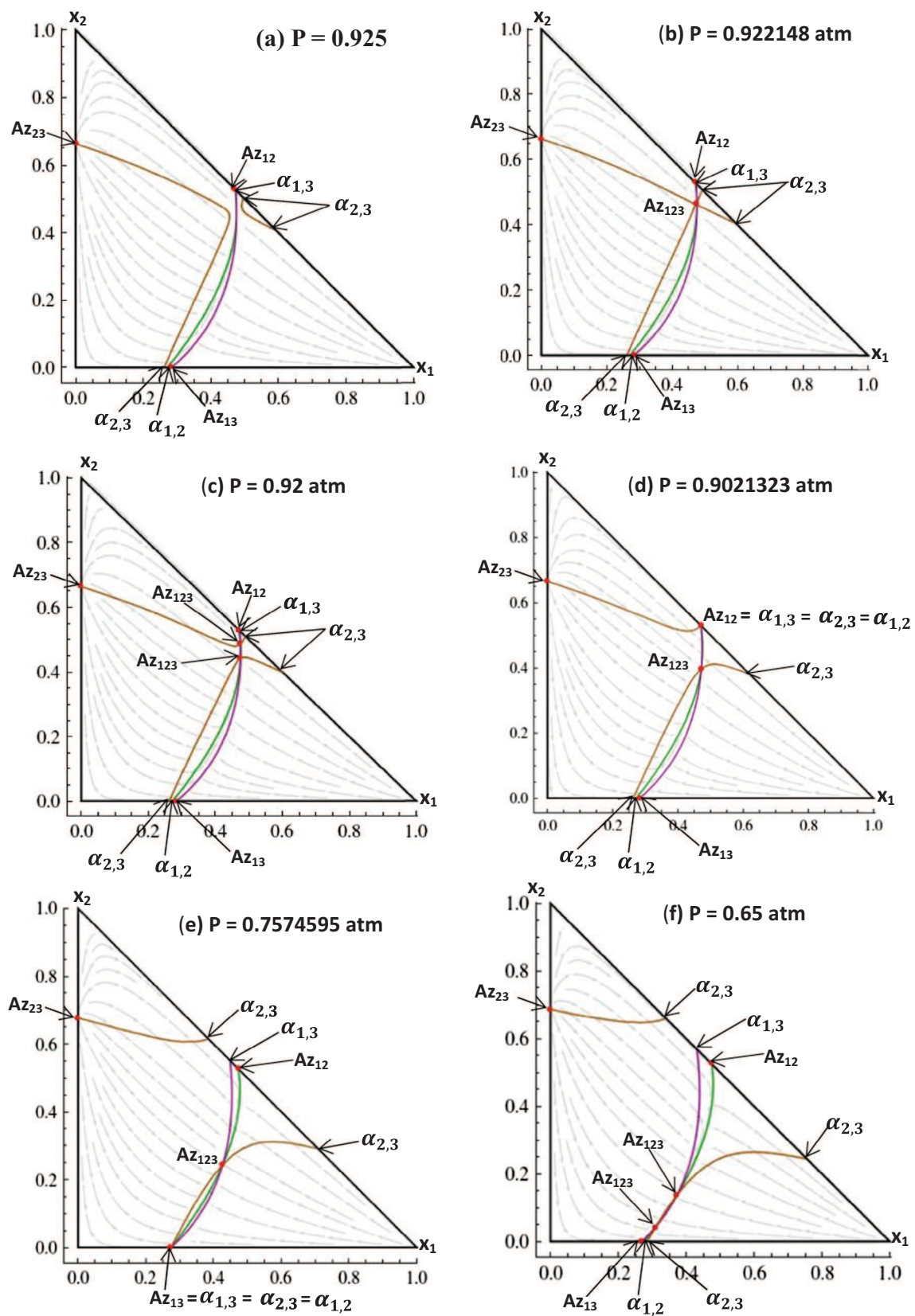
Fig. 5. RCM and univolatility curves of the mixture diethylamine(1) – chloroform (2) – methanol (3) at different pressures.
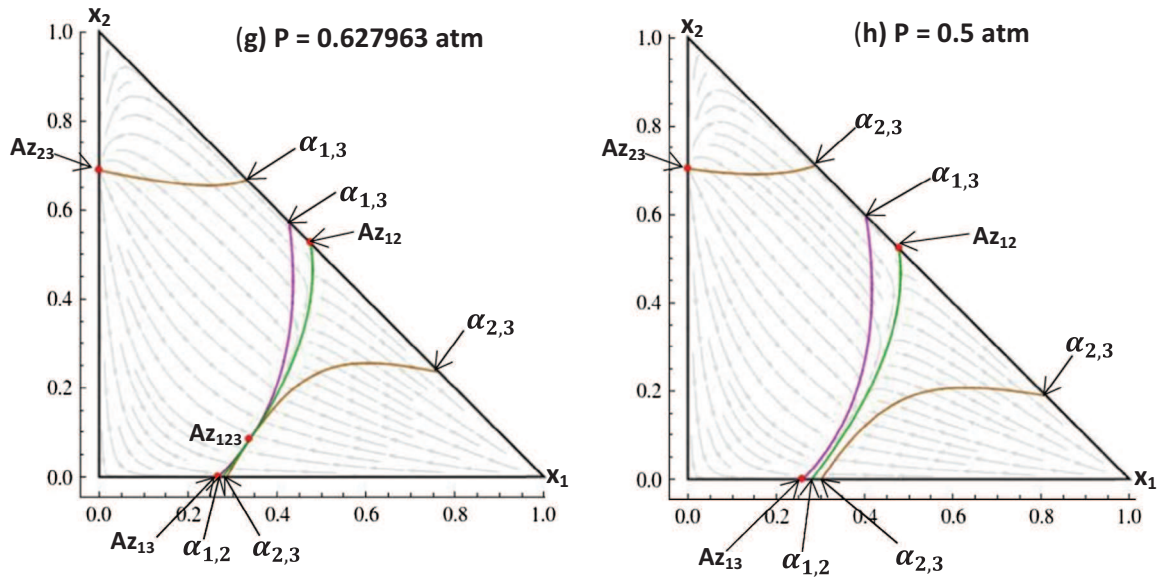
Fig. 5 (*continued*)

3.2. Case Study: hexane (1) – benzene (2) – hexafluorobenzene (3)

As it is shown in Fig. 7, at the reference pressure 1 atm, the RCM of this ternary mixture has two binary azeotropes Az^*_{23} (saddle) and Az^{**}_{23} (stable node) on the binary side benzene (2) – hexafluorobenzene (3). The other two binary azeotropes belong to the sides benzene (2) – hexane (1) and hexafluorobenzene (3) – hexane (1). The RCM is characterized by four univolatility curves issued from each of the binary azeotropes. In addition, the univolatility curve $\alpha_{2,3} = 1$ is composed by two branches of $\overline{\overline{\alpha_{i,j}}}$ – type. As shown in the right-hand side of Fig. 7, the terminal points of both curves $\overline{\overline{\alpha_{2,3}}}$ on the binary edge hexane (1) – benzene (2) can be detected by the double intersection between the distribution curve of $k_3^{\infty 1,2}$ with the curve for $k_2^{1,2}$. The pair of binary azeotropes on the 2–3 edge comes from the double simultaneous intersection of the distribution curves $k_2^{2,3}$ and $k_3^{2,3}$ with the unit level curve.

The pressure increase allows tracing out some peculiar transformations of the topological structure of the RCM of this mixture. First of all, at P ≈ 1.07705 atm, two branches $\overline{\overline{\alpha_{2,3}}}$ join to form a unique cross shape univolatility curve, as shown in Fig. 8a. A similar configuration was observed in Fig. 5b. This phenomenon corresponds to the existence of the common tangent point of the boiling temperature surface and the univolatility hypersurface, as shown in Fig. 10. Unlike to the case presented in Fig. 5b, here the singularity of the univolatility curve is not related to the existence of the ternary azeotrope. In fact, this singular point is not a critical point of the boiling temperature T_b, and hence the boiling temperature surface W intersects the other two univolatility hypersurfaces $\Psi_{12} = 0$ and $\Psi_{13} = 0$ far from this point. With the further increment of pressure (Fig. 8b) the two branches of the curve $\alpha_{2,3} = 1$ split into two curves of $\overline{\alpha_{i,j}}$-type. Such a transformation cannot be detected from the analysis of the distribution curves $k_m^{\infty i,j}$, $k_i^{i,j}$ and $k_j^{i,j}$. Indeed, the distribution curves diagrams at P = 1 atm (Fig. 7) and at P = 1.2 atm (Fig. 9) are almost identical. Remarkably, one of the new univolatility curves (labelled $\alpha^*_{2,3}$) connects two binary azeotropes Az^*_{23} and Az^{**}_{23}. With the further pressure growth, the

binary azeotrope Az_{12} disappears together with the univolatility curve $\alpha_{1,2} = 1$ and the right branch of the curve $\alpha_{2,3} = 1$. The two azeotropes Az^*_{23} and Az^{**}_{23} move closer making the curve $\alpha^*_{2,3}$ shorter and closer to the edge 2–3. At P ≈ 4.93806 atm (Fig. 11) Az^*_{23} and Az^{**}_{23} join to form a singular binary azeotrope, which is not connected to any univolatility curve. This point corresponds to the only common point between the boiling temperature surface and the hypersurface defined by $\Psi_{23} = 0$ in the tree-dimensional state space. With the further pressure increase, this azeotrope disappears and $\alpha_{1,3} = 1$ remains the only univolatility curve of the ternary mixture.

4. Conclusion

The feasibility of the separation and the design of distillation units can be assessed by the analysis of residue curve maps (RCMs) and univolatility and unidistribution curves. Kiva et al. (2003) reviewed their properties and interdependence. The topology of RCMs and of univolatility curve maps is not trivial even in the case of ternary mixtures, as is known from Serafimov's and Zhvanetskii's classifications (1988, 1990). These classifications are usually shown in the two dimensional composition space. However, the two dimensional representation does not reflect the true nature of the univolatility curves.

In this paper, we propose a novel method allowing the detection of the univolatility curves in homogeneous ternary mixtures independently of the presence of the azeotropes, which is particularly important in the case of zeotropic mixtures. The method is based on the analysis of the geometry of the boiling temperature surface constrained by the univolatility condition. We have demonstrated that the curves where $\alpha_{i,j} = 1$ are the loci of critical points of the relative compositions x_j/x_i. We proposed a simple method for efficient computation of univolatility curves by solving an initial value problem. The starting points are found by using the intersection of the distribution coefficient curve $k_m^{\infty i,j}$ with the curves $k_i^{i,j}$, of $k_j^{i,j}$ along each binary side *i-j* of the composition triangle, where the component *m* is considered at infinite dilution.
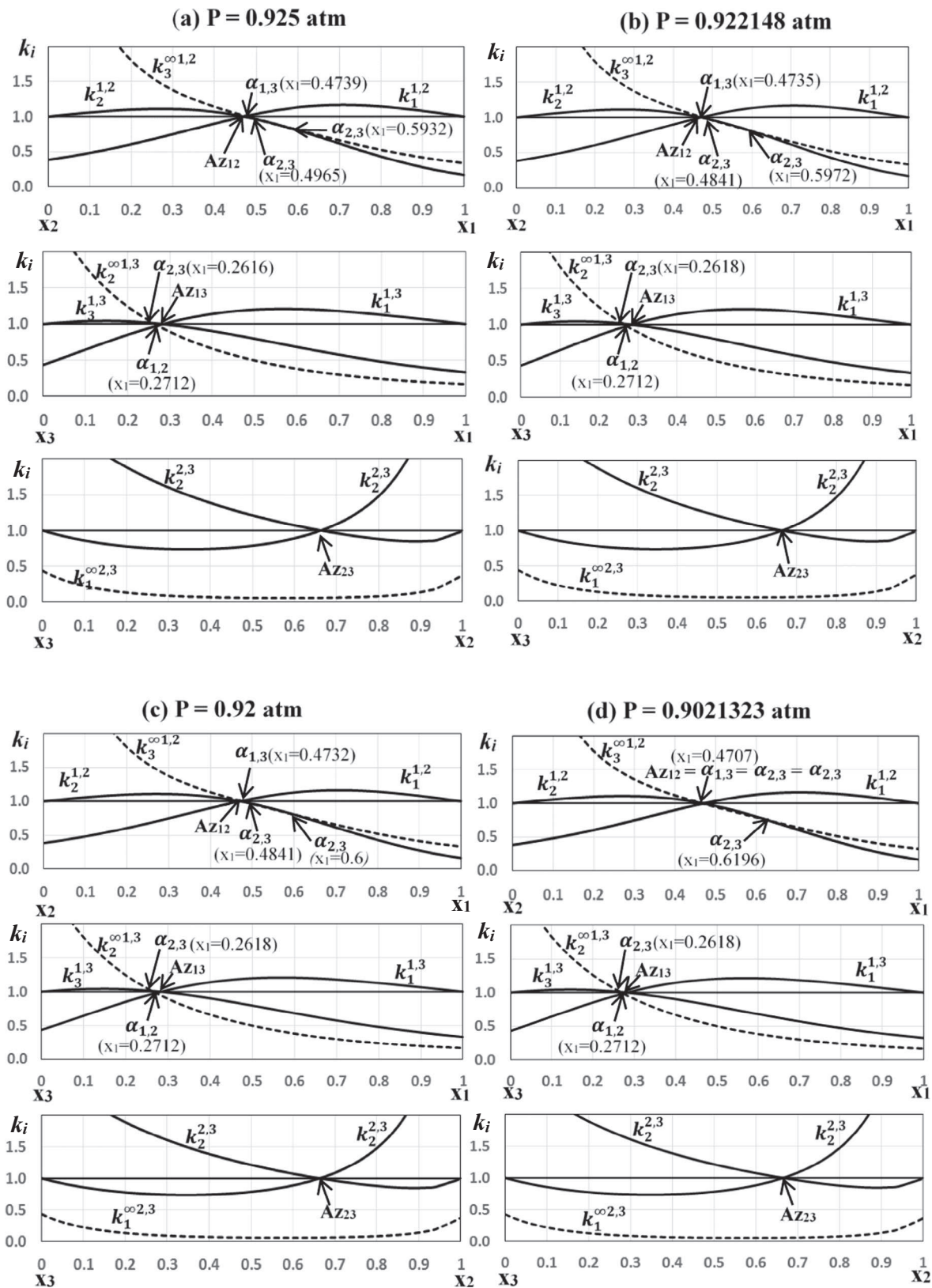
Fig. 6. Distribution curves on each binary edges 1–2, 1–3 and 2–3 of the mixture diethylamine (1) – chloroform (2) – methanol (3) at different pressures.

(e) P = 0.7574595 atm

(f) P = 0.65 atm
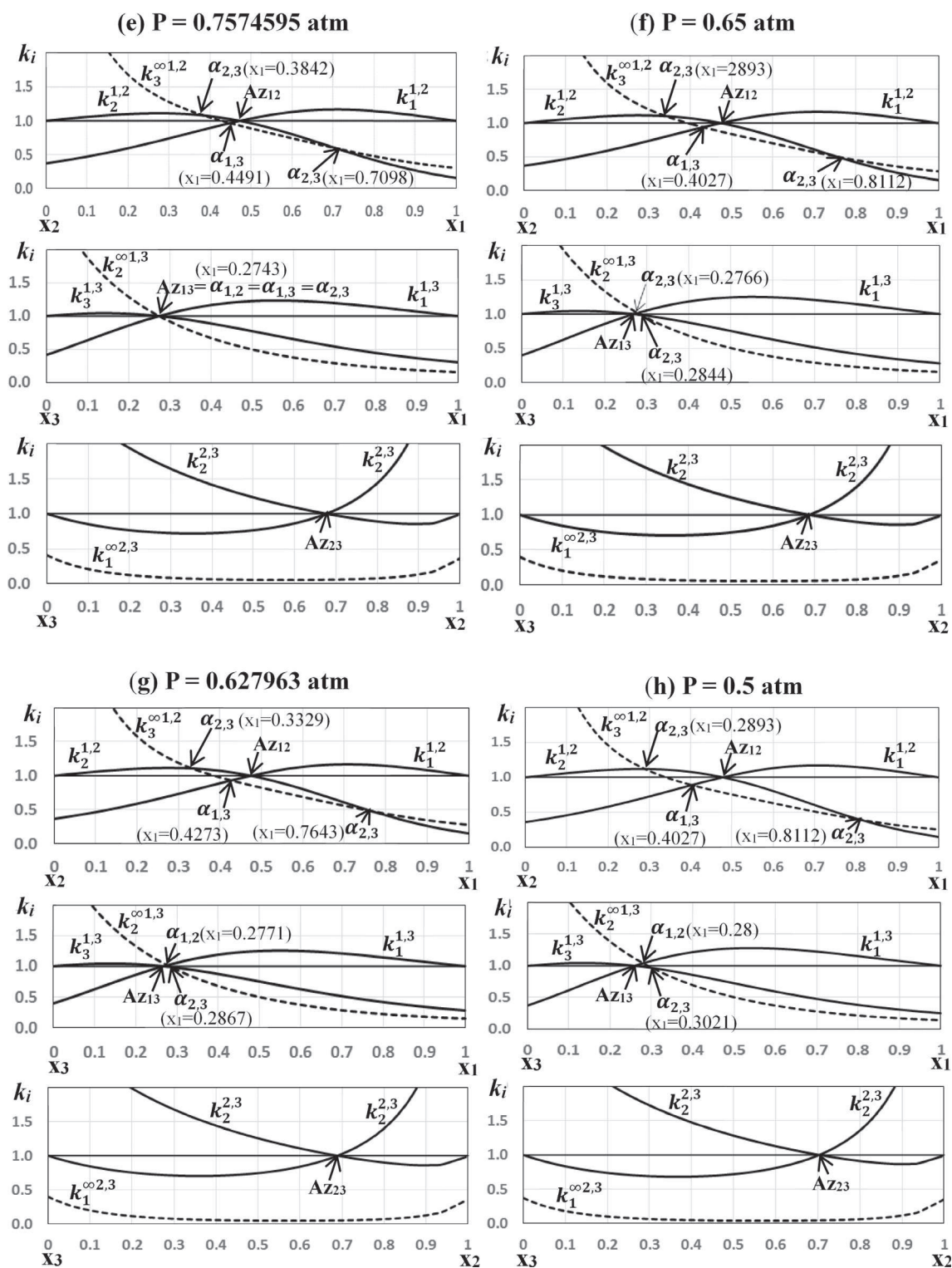
(g) P = 0.627963 atm

(h) P = 0.5 atm

Fig. 6 (*continued*)

Two peculiar ternary systems, namely diethylamine – chloroform – methanol and hexane – benzene – hexafluorobenzene were used for illustration of the unusual univolatility curves starting and ending on the same binary side. By varying the pressure, we also observed a rare occurrence of tangential azeotropes, saddle-node

ternary azeotropes and bi-ternary and bi-binary azeotropy phenomena. In both examples, a transition cross-shape univolatility curve appears as a consequence of existence of a common tangent point between the three dimensional univolatility hypersurface and the boiling temperature surface. The same computations were
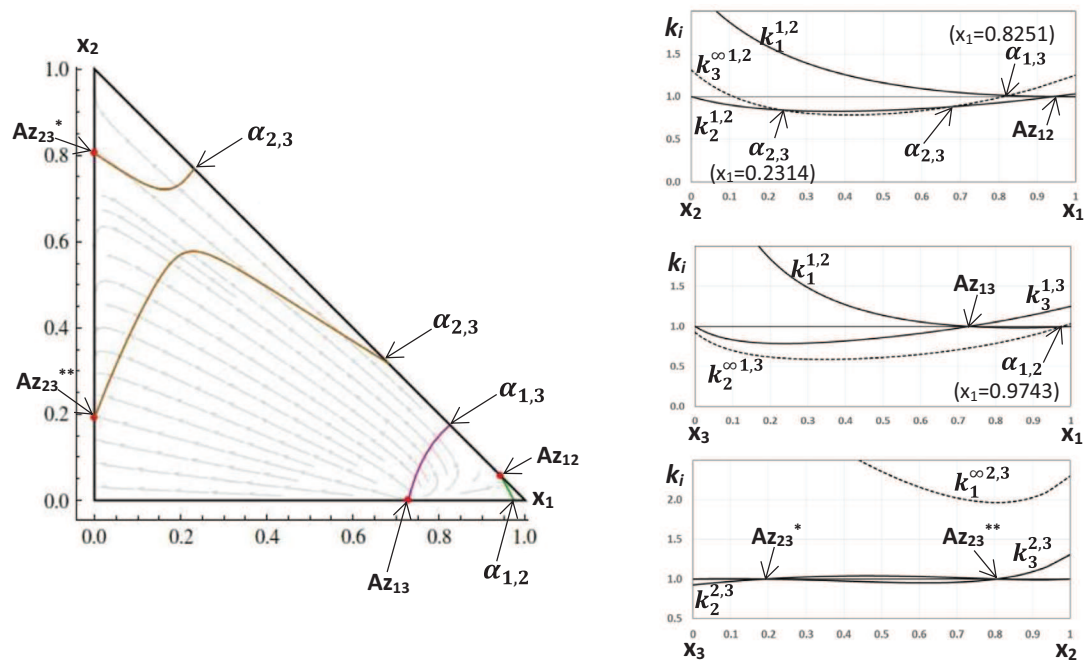
Fig. 7. RCM, univolatility curves and distribution curves on the binary edges 1–2, 1–3 and 2–3 for the mixture hexane (1) – benzene (2) – hexafluorobenzene (3). P = 1 atm.
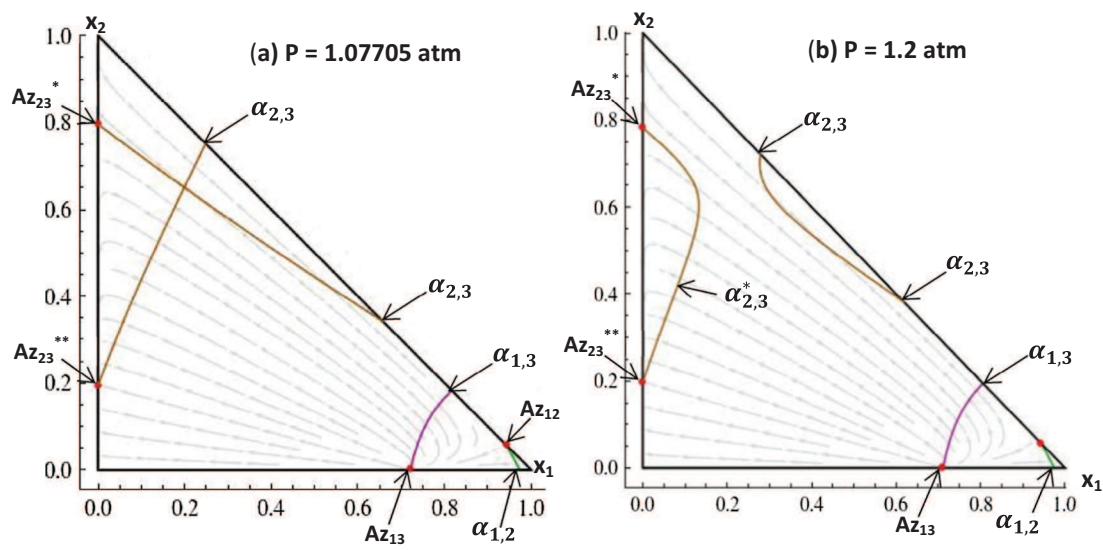

Fig. 8. RCM, univolatility curves on the binary edges 1–2, 1–3 and 2–3 for the mixture mixture hexane (1) –benzene (2) – hexafluorobenzene (3) at different pressures.
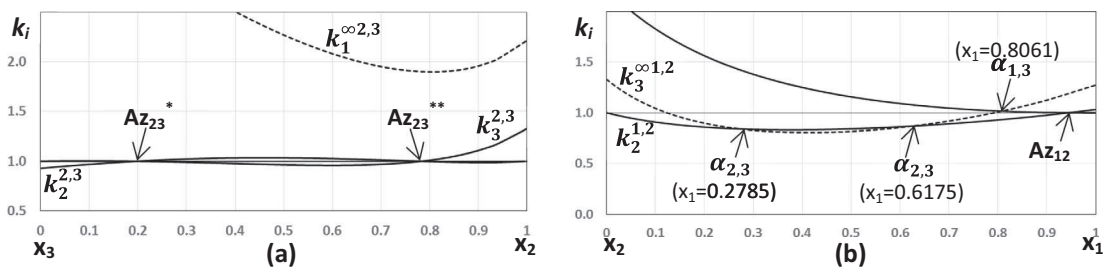

Fig. 9. Distribution curves on the binary edges (a) 2–3 and (b) 1–2 for the mixture hexane (1) – benzene (2) – hexafluorobenzene (3) at P = 1.2 atm.
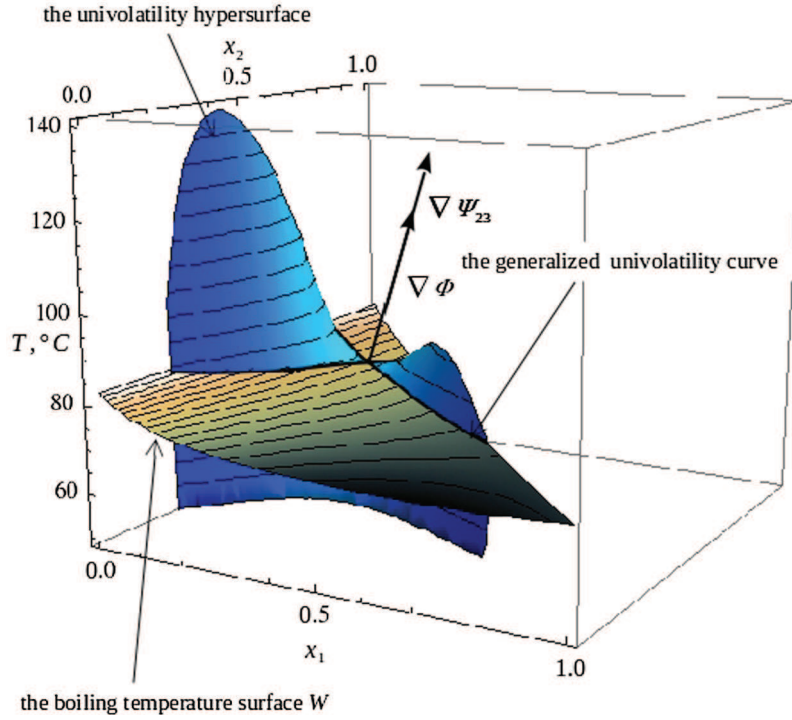
Fig. 10. Mixture hexane (1) – benzene (2) – hexafluorobenzene (3): the mutual arrangement of the boiling temperature surface and the univolatility hypersurface $\Psi_{23} = 0$ at $P \approx 1.07705$ atm.
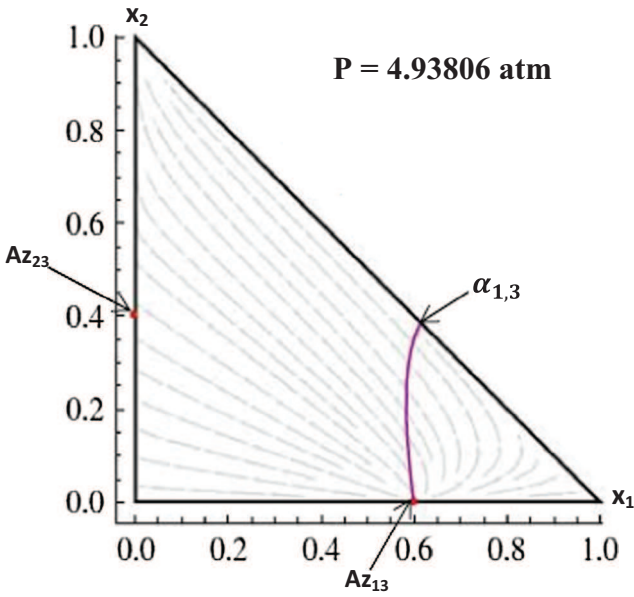

Fig. 11. RCM and univolatility curves of the mixture hexane (1) – benzene (2) – hexafluorobenzene (3) at $P \approx 4.93806$ atm.

performed using Aspen Plus V 8.6 with built-in NRTL binary coefficients database for both ternary mixtures: diethylamine – chloroform - methanol mixture and hexane – benzene – hexafluorobenzene. In contrast to our results, these computations failed for all univolatility curves non-connected to azeotropic compositions at the fixed pressure.

Appendix A. Derivation of Eqs. (6) and (7)

Consider a residue curve $\beta(\xi) = (x_1(\xi), x_2(\xi))$ in Ω and the univolatility curve $\alpha_{1,2} = 1$. We have:

$$
\begin{aligned}
(k_1 - k_2)|_{\bar{x} \in \beta(\xi)} &= \frac{y_1}{x_1} - \frac{y_2}{x_2} = \frac{y_1 x_2 - y_2 x_1}{x_1 x_2} = \frac{y_1 x_2 - y_2 x_1 + x_1 x_2 - x_1 x_2}{x_1 x_2} \\
&= \frac{(x_2 - y_2)x_1 - (x_1 - y_1)x_2}{x_1 x_2}
\end{aligned}
\tag{A.1}
$$

By definition, β is a solution to Eq. (3), which in vector form is expressed as $\dot{\bar{x}} = \bar{v} = (x_1 - y_1, x_2 - y_2)$, where "·" means the derivative with respect to the dimensionless parameter ξ. Hence

$$
\begin{aligned}
(k_1 - k_2)|_{\bar{x} \in \beta(\xi)} &= \frac{v_2 x_1 - v_1 x_2}{x_1 x_2} = \frac{\dot{x}_2 x_1 - \dot{x}_1 x_2}{x_1 x_2} = \frac{\dot{x}_2}{x_2} - \frac{\dot{x}_1}{x_1} \\
&= \frac{d}{d\xi}\left(\ln \frac{x_2}{x_1}\right)
\end{aligned}
\tag{A.2}
$$

which completes the proof of Eq. (6). We also remark that in vector notation the right-hand side of Eq. (A.1) can be rewritten as a wedge product of the vectors $\bar{x}$ and $\bar{v}$:

$$
(k_1 - k_2)|_{\bar{x} \in \beta(\xi)} = \frac{v_2 x_1 - v_1 x_2}{x_1 x_2} = \frac{\bar{x} \wedge \bar{v}}{x_1 x_2}
$$

The differentiation of Eq. (A.2) with respect to ξ yields:

$$\frac{d}{d\xi}(k_1 - k_2)\Big|_{\bar{x}\in\beta(\xi)} = \frac{\ddot{x}_2}{x_2} - \frac{\ddot{x}_1}{x_1} - \frac{\dot{x}_2^2}{x_2^2} + \frac{\dot{x}_1^2}{x_1^2}$$

$$= \frac{\ddot{x}_2 x_1 - \ddot{x}_1 x_2}{x_1 x_2} - \left(\frac{\dot{x}_2}{x_2} - \frac{\dot{x}_1}{x_1}\right)\left(\frac{\dot{x}_1}{x_1} + \frac{\dot{x}_2}{x_2}\right) \qquad (A.3)$$

$$= \frac{\ddot{x}_2 x_1 - \ddot{x}_1 x_2}{x_1 x_2} - (k_1 - k_2)\frac{v_1 x_2 + v_2 x_1}{x_1 x_2}$$

which in vector notation becomes Eq. (7):

$$\frac{d}{d\xi}(k_1 - k_2)\Big|_{\bar{x}\in\beta(\xi)} = \frac{\bar{x}\wedge\ddot{\bar{x}}}{x_1 x_2} - (k_1 - k_2)\frac{v_1 x_2 + v_2 x_1}{x_1 x_2}$$

Appendix B. Surfaces in the three-dimensional space

Consider a three dimensional space $\mathbb{R}^3$ and let (x, y, z) be the standard Cartesian coordinates in it. Let $F : \mathbb{R}^3 \to \mathbb{R}$ be a smooth (at least twice continuously differentiable) function. The implicit equation $F(x, y, z) = 0$ defines a *hyper-surface* (or just *surface*) in $\mathbb{R}^3$. This surface is *regular* at a point $P \in \mathbb{R}^3$ if the gradient $\nabla F(P) = \left(\frac{\partial F}{\partial x}, \frac{\partial F}{\partial y}, \frac{\partial F}{\partial z}\right)(P)$ is different from zero. According to the Implicit Function Theorem if $\frac{\partial F}{\partial z}(P) \neq 0$, the implicit equation $F(x, y, z) = 0$ can be solved with respect to z in the neighborhood of P. In other words, the surface can be presented on the form $z = f(x, y)$, i.e. as a graph of a smooth function $f : \mathbb{R}^2 \to \mathbb{R}$.

Assume that the surface W described implicitly by F is regular. Consider a smooth curve $\gamma(t) = (x(t), y(t), z(t))$ on W by assuming that $F(x(t), y(t), z(t)) = 0$. Differentiating with respect to t yields:

$$\frac{\partial F}{\partial x}\frac{dx}{dt} + \frac{\partial F}{\partial y}\frac{dy}{dt} + \frac{\partial F}{\partial z}\frac{dz}{dt} = 0$$

Here the vector $v = \left(\frac{dx}{dt}, \frac{dy}{dt}, \frac{dz}{dt}\right)$ defines the tangent vector to the curve at a point $P = (x, y, z)$. The set of all tangent vectors of all curves passing through the point P defines the two-dimensional *tangent plane* to W at P. It is now easy to see that the vector $\nabla F(P) = (\frac{\partial F}{\partial x}, \frac{\partial F}{\partial y}, \frac{\partial F}{\partial z})(P)$ is orthogonal to the tangent plane, i.e. it defines *the normal vector* N_W to W at P.

Appendix C. Supplementary material

Supplementary data associated with this article can be found, in the online version, at http://dx.doi.org/10.1016/j.ces.2017.07.007.

References

Arlt, W., 2014. Azeotropic distillation (Chapter 7). In: Gorak, A., Olujic, Z. (Eds.), Distillation Book, Distillation: Equipment and Processes, vol. II. Elsevier, Amsterdam, pp. 247–259. ISBN 978-0-12-386878-7.

Bogdanov, V.S., Kiva, V.N., 1977. Localization of single [Unity] K- and -lines in analysis of liquid-vapor phase diagrams. Russ. J. Phys. Chem. 51 (6), 796–798.

Do Carmo, M., 1976. Differential Geometry of Curves and Surfaces. Prentice-Hall, New Jersey, p. 503.

Doherty, M.F., Malone, M.F., 2001. Conceptual Design of Distillation Systems. McGraw-Hill, New York.

Gerbaud, V., Rodriguez-Donis, I., 2014. Extractive distillation (Chapter 6). In: Gorak, A., Olujic, Z. (Eds.), Distillation Book, Distillation: Equipment and Processes, vol. II. Elsevier, Amsterdam, pp. 201–246. ISBN 978-0-12-386878-7.

Hilmen, E.K., Kiva, V.N., Skogestad, S., 2002. Topology of ternary VLE diagrams: elementary cells. AIChE J. 48 (4), 752–759.

Ji, G., Liu, G., 2007. Study on the feasibility of split crossing distillation compartment boundary. Chem. Eng. Process. 46, 52–62.

Jordan, I.N., Temenujka, K.S., Peter, S.P., 1985. Vapor-liquid equilibria at 101.3 kPa for diethylamine + chloroform. J. Chem. Eng. Data 40, 199–201.

Kiss, A.A., 2014. Distillation technology – still young and full of breakthrough opportunities. J. Chem. Technol. Biotechnol. 89, 479–498.

Kiva, V.N., Hilmen, E.K., Skogestad, S., 2003. Azeotropic phase equilibrium diagrams: a survey. Chem. Eng. Sci. 58, 1903–1953.

Kiva, V.N., Serafimov, L.A., 1973. Non-local rules of the movement of process lines for simple distillation in ternary systems. Russ. J. Phys. Chem. 47 (3), 638–642.

Lang, S., 1987. Calculus of Several Variables,. .. Undergraduate Texts in Mathematics, third ed. Springer Science + Business Media.

Laroche, L., Bekiaris, N., Andersen, H.W., Morari, M., 1991. Homogeneous azeotropic distillation: comparing entrainers. Can. J. Chem. Eng. 69, 1302–1319.

Lelkes, Z., Lang, P., Otterbein, M., 1998. Feasibility and sequencing studies for homoazeotropic distillation in a rectifier with continuous entrainer feeding. Comp. Chem. Eng. 22, S653–656.

Luyben, W.L., Chien, I.-L., 2010. Design and Control of Distillation Systems for Separating Azeotropes. John Wiley & Sons, Hoboken, New Jersey.

Olujic, Z., 2014. Vacuum and High-pressure distillation (Chapter 9). In: Gorak, A., Olujic, Z. (Eds.), Distillation Book, Distillation: Equipment and Processes, vol. II. Elsevier, Amsterdam, pp. 295–318. ISBN 978-0-12-386878-7.

Petlyuk, F.B., 2004. Distillation Theory and its Application to Optimal Design of Separation Units. Cambridge University Press, New York.

Petlyuk, F., Danilov, R., Burger, J., 2015. A novel method for the search and identification of feasible splits of extractive distillations in ternary mixtures. Chem. Eng. Res. Des. 99, 132–148.

Reshetov, S.A., Kravchenko, S.V., 2007a. Statistics of liquid-vapor phase equilibrium diagrams for various ternary zeotropic mixtures. Theor. Found. Chem. Eng. 41 (4), 451–453.

Reshetov, S.A., Kravchenko, S.V., 2007b. Statistics of liquid-vapor phase equilibrium diagrams for various ternary zeotropic mixtures. Theor. Found. Chem. Eng. 44 (3), 279–292.

Reshetov, S.A., Kravchenko, S.V., 2010. Statistical analysis of the kinds of vapor-liquid equilibrium diagrams of three-component systems with binary and ternary azeotropes. Theor. Found. Chem. Eng. 41 (4), 451–453.

Reshetov, S.A., Sluchenkov, V.Yu., Ryzhova, V.S., Zhvanetskii, I.B., 1990. Diagrams of K-ordered regions with an arbitrary number of unitary α-lines. Russ. J. Phys. Chem. [Zh. Fiz. Khim.] 64 (9), pp. 1344–1347 and 2498–2503.

Rodriguez-Donis, I., Gerbaud, V., Joulia, X., 2009a. Thermodynamic insights on the feasibility of homogeneous batch extractive distillation. 1. Azeotropic mixtures with heavy entrainer. Ind. Eng. Chem. Res. 48 (7), 3544–3559.

Rodriguez-Donis, I., Gerbaud, V., Joulia, X., 2009b. Thermodynamic insights on the feasibility of homogeneous batch extractive distillation. 2. Low-relative-volatility binary mixtures with a heavy entrainer. Ind. Eng. Chem. Res. 48, 3560–3572.

Rodriguez-Donis, I., Gerbaud, V., Joulia, X., 2012a. Thermodynamic insights on the feasibility of homogeneous – batch extractive distillation. 3. Azeotropic mixtures with light entrainer. Ind. Eng. Chem. Res. 51 (12), 4643–4660.

Rodriguez-Donis, I., Gerbaud, V., Joulia, X., 2012b. Thermodynamic insights on the feasibility of homogeneous batch extractive distillation. 4. Azeotropic mixtures with intermediate boiling entrainer. Ind. Eng. Chem. Res. 51 (12), 6489–6501.

Skiborowski, M., Harwardt, A., Marquardt, W., 2014. Conceptual design of azeotropic distillation processes (Chapter 8). In: Gorak, A., Sorensen, E. (Eds.), Distillation Book, Distillation: Fundamentals and Principles, vol. I. Elsevier, Amsterdam, pp. 305–355. ISBN 978-0-12-386574-2.

Skiborowski, M., Bausa, J., Marquardt, W., 2016. A Unifying approach for the calculation of azeotropes and pinch points in homogeneous and heterogeneous mixtures. Ind. Eng. Chem. Res. 55, 6815–6834.

Wahnschafft, O.M., Westerberg, A.W., 1993. The product composition regions of azeotropic distillation columns. 2. Separability in two-feed column and entrainer selection. Ind. Eng. Chem. Res. 32, 1108–1120.

Widagdo, S., Seider, W.D., 1996. Azeotropic distillation. AIChE J. 42, 96–126.

Zhvanetskii, I.B., Reshetov, S.A., Sluchenkov, V., 1988. Classification of the K-order regions on the distillation line diagram for a ternary zeotropic system. Russ. J. Phys. Chem. 62 (7), pp. 996–998 and 1944–1947.